Chemical Engineering Journal 279 (2015) 861–873

Contents lists available at ScienceDirect

Chemical Engineering Journal

journal homepage: www.elsevier.com/locate/cej

Naproxen abatement by thermally activated persulfate in aqueous systems

Antoine Ghauch *, Al Muthanna Tuqan, Nadine Kibbi

American University of Beirut, Faculty of Arts and Sciences, Department of Chemistry, P.O. Box 11-0236, Riad El Solh, 1107-2020 Beirut, Lebanon

HIGHLIGHTS

- Naproxen is fully degraded in thermally activated persulfate systems.
- Naproxen degradation mechanism is highly dependent on $SO_4^{\cdot-}$ rather than on $OH^{\cdot}$ radicals.
- Naproxen mineralization extent is proportional to persulfate concentration.
- Inorganic ions slightly affect naproxen degradation efficiency in TAP systems.
- TAP systems showed total mineralization of naproxen in highly charged hospital effluent.

ARTICLE INFO

Article history:
Received 4 February 2015
Received in revised form 16 May 2015
Accepted 20 May 2015
Available online 27 May 2015

Keywords:
Naproxen
Advanced oxidation processes
Hospital effluent
Decontamination
Water reuse

ABSTRACT

In this work, we investigated the use of thermally activated persulfate (TAP) as one of the most powerful advanced oxidation processes for the treatment of pharmaceuticals present in effluents. Pilot experiments were carried out on naproxen (NAP) solutions, and the effect of experimental conditions (e.g. inorganic additives, matrix) was assessed so as to better evaluate TAP systems and improve the reaction stoichiometric efficiency. A comparative kinetics study was provided for the removal of NAP vs work previously published using however other classes of pharmaceuticals e.g. bisoprolol, ibuprofen. The activation energy (E_A) calculated was found to be 155.03 (±26.4) kJ mol^{-1}. The best degradation rate was observed at 70 °C and found to be equal to 1.286×10^{-4} mM min^{-1}. Furthermore, experiments were performed on untreated hospital effluents collected from the largest hospital in Beirut and spiked with NAP solution (50 μM). Results showed full mineralization of the pharmaceutical effluent that was achieved and monitored via total organic carbon (TOC) analysis. Liquid and gas chromatography coupled with mass spectrometry were the techniques used for the identification of NAP and its transformation products. A NAP degradation mechanism was proposed and found to be mainly based on the action of sulfate radicals operating by electron abstraction. This study demonstrated once more that TAP systems are a valid and efficient method that can be used for the removal of dissolved pharmaceuticals in water and sewage water.

1. Introduction

In recent years, non-steroidal anti-inflammatory drugs (NSAIDs) have been found in water effluents in increasing concentrations e.g. ng L^{-1} to μg L^{-1} [1,2]. The issue obtained growing interest because of the potential threats that NSAIDs cause to both the ecological system and human beings [3,4]. In this study, we have chosen naproxen (NAP) for its presence in sewage treatment plant effluents and drinking water in significant concentrations 17–313 ng L^{-1} [1]. NAP toxicity was not only reported on bacteria, microcrustaceans and algae, but also on humans [5]. It was also reported that people who ingest trace amounts of NAP for a long time may have a higher risk of having a heart attack or a stroke than people who are not exposed to this medication [6]. In the past few years, several studies have been conducted on the subject of NAP removal from water. These studies used different treatment methods and remediation technologies such as photo-degradation, ozonation, ultra-sonication, gamma irradiation, nanofiltration [7–13]. Benitez et al. [14] showed that O_3/H_2O_2 was the most successful oxidative system for NAP (1 μM) degradation in ultrapure water (UP) with an achieved degradation rate of about 2.64×10^{-4} M^{-1} s^{-1}. Two years later, Marotta et al. [10] investigated the role of oxygen during photo-degradation of NAP solution

* Corresponding author. Tel.: +961 1350 000; fax: +961 1 365 217.
E-mail address: antoine.ghauch@aub.edu.lb (A. Ghauch).

http://dx.doi.org/10.1016/j.cej.2015.05.067
1385-8947/

(1 μM) and found better results in oxic solutions rather than under anaerobic conditions. In 2014, Ma et al. [7] demonstrated that NAP (43 μM) photo-degradation by direct solar photolysis and by self-sensitization via reactive oxygen species was effective. However, the adopted process yielded some intermediate products more toxic than NAP. In 2015, Rein and Welch [15] found that NAP's photo-degradation products were significantly more toxic than NAP itself, and combinations of NAP and its photo-degradation products were particularly toxic. Accordingly, investigations into new methods of NAP's removal become of interest, especially if the resulting transformation products are more biodegradable, totally absent or at least do not represent greater toxicity than NAP, the parent NSAID [15].

Since several methods have been developed to remove pharmaceuticals from water effluents [16], the focus has also been toward efficient and economically viable techniques, especially for large scale treatment and field applications. Persulfate technology emerged in the recent years as part of the advanced oxidation processes (AOPs) to be considered by water treatment specialists [17,18].

In the past decade, TAPs have been significantly applied as powerful in situ chemical oxidation (ISCO) processes for the removal of volatile organic compounds [19], polycyclic aromatic hydrocarbons (PAHs) [20], trichloroethylene [21] and very recently pharmaceuticals [22–25] and dyes [26,27] in water. When used for ISCO processes sodium persulfate (PS) showed very promising results due to its high redox potential (Eq. (1)) and its strongly oxidative sulfate radical $SO_4^{\cdot-}$ (Eq. (2)) that can either be generated thermally or chemically (Eqs. (3)–(5)) [28,29]. In thermally activated systems, increased temperatures result in faster generation of the oxidative $SO_4^{\cdot-}$ [22,23], while in chemically activated systems, excess of activators might jeopardize the oxidation process due to $SO_4^{\cdot-}$ quenching [24,25,30]:

$$S_2O_8^{2-} + 2e \rightarrow 2SO_4^{2-} \text{ with } E^0 = 2.01 \text{ V/SHE} \quad (1)$$

$$SO_4^{\cdot-} + e \rightarrow SO_4^{2-} \text{ with } E^0 = 2.41 \text{ V/SHE} \quad (2)$$

$$S_2O_8^{2-} \rightarrow 2SO_4^{\cdot-} \text{ (Thermal activation) with } 30\,^{\circ}C < T < 99^{\circ} \quad (3)$$

$$S_2O_8^{2-} + Fe^{2+} \rightarrow SO_4^{2-} + SO_4^{\cdot-} + Fe^{3+} \text{ (Chemical activation)} \quad (4)$$

$$SO_4^{\cdot-} + Fe^{2+} \rightarrow SO_4^{2-} + Fe^{3+} \text{ with } k = 4.6 \times 10^9\ M^{-1}\ s^{-1} \quad (5)$$

To our knowledge, no data exists today on the removal of NAP from water in TAP systems especially when it comes to highly charged effluents e.g. hospitals, clinical laboratories, etc. In the present study, TAP systems are adopted in order to investigate NAP degradation in UP water as well as in a hospital effluent (HE). A kinetics study is presented taking into account the reaction rate and reaction stoichiometric efficiencies (RSEs) under controlled temperatures (40–70 °C) and in the presence of inorganic additives at circumneutral pH. Scavenging reactions are performed as well to identify the main oxidative radical ($SO_4^{\cdot-}$ vs $HO^{\cdot}$). The calculated activation energy (E_A) of NAP is determined and compared to that of other pharmaceuticals previously investigated under similar conditions [22,23]. TOC analyses are performed on treated solutions demonstrating full NAP mineralization. At the end, an assessment of TAP systems for the removal of dissolved pharmaceuticals in a real HE collected from the effluent of the largest hospital located in Beirut is presented. NAP transformation products are identified and a degradation mechanism is proposed.

2. Materials and methods

2.1. Chemicals

Pharmaceutical grade naproxen sodium (NAP), sodium persulfate (PS) ($Na_2S_2O_8$, 99+%) and acetic acid glacial (CH_3COOH, 99.5+%) were purchased from Sigma–Aldrich (China), Chem-Lab (Belgium) and Surechem Products LTD (UK), respectively. Sodium dihydrogen phosphate dihydrate ($NaH_2PO_4{\cdot}2H_2O$, 99+%) and disodium hydrogen phosphate (Na_2HPO_4, 99+%) were acquired from Fluka (Netherlands) and Merck (Germany), respectively. Potassium iodide (KI) (puriss, 99–100.5%) and potassium dihydrogen phosphate (KH_2PO_4) were obtained from Riedel-de-Haen (Germany). Acetonitrile (CH_3CN) and methanol (CH_3OH) were both of HPLC grade and purchased from Sigma (USA).

2.2. Chemical analysis

2.2.1. HPLC/DAD/FLD/MSD

NAP was analyzed using an Agilent 1100 Series high pressure liquid chromatography (HPLC). The HPLC system is composed of a quaternary pump equipped with a vacuum degasser, thermostated autosampler and column compartment in addition to a diode array detector (DAD) and a fluorescence detector (FLD). Both were placed in series with an ion-trap mass spectrometry detector (MSD). A C_{18} reverse phase column (5 μm; 4.6 i.d. × 250 mm long) attached to a pre-column guard HS C_{18} (5 μm; 4.6 i.d. × 20 mm long, Discovery, Supleco, USA) was used for the separation of pharmaceutical molecules and all derivatives. Both column and column guard were maintained at 30 °C throughout the analysis. The mobile phase consisted of acetonitrile (55%) and 0.04% (v/v) acetic acid glacial (45%) percolating through the column in an isocratic mode with a flow rate of 1.0 mL min^{-1}. The sample injection volume was about 50 μL. The whole chromatography system was controlled by Agilent ChemStation software for LC and LC/MS systems version A.09.0.

For HE samples, the same HPLC system was used however with gradient elution in order to better separate dissolved organic molecules inside. The mobile phase was composed of (A) 50 mM KH_2PO_4 and (B) acetonitrile. The gradient was run as follows: at time 0–4.5 min, 85% of (A) and 15% of (B); at t = 12.5 min, 80% of (A) and 20% of (B); at t = 18 min, 75% of (A) and 25% of (B); finally at t = 27–45 min, 55% of (A) and 45% of (B).

2.2.2. GC/MS

MS analyses were performed on a thermo scientific GC/MS equipped with a POLARIS Q Ion Trap MS detector, a Thermo Finnigan autosampler and XCalibur software (USA) in order to identify NAP transformation products. The conditions were as follows: EI = 70 eV, manifold temperature 473 K, dwell time 100 μs and scan range of 50–500 m/z. Separation was done on Agilent DB-23 column (30 m length, 0.25 mm internal diameter and 0.25 μm film thickness) flushed with Helium as carrier gas. The injection volume was about 2 μL. System temperature was programed to start at 373 K for 2.5 min followed by a 6 K/min increase up to 523 K then held for 15 min.

2.2.3. Persulfate analysis

Persulfate anion concentration was determined on a Nanodrop 2000c UV–vis spectrophotometer (Thermo scientific) as per the procedure developed by Liang et al. [31]. The absorbance of the complex was measured at λ = 352 nm. PS calibration curves were performed with a range of concentrations of 5–1000 μM (Fig. 1S). The limit of detection of PS under these conditions was less than 5.0 μM [22,23].

2.2.4. Total organic carbon

TOC measurements were conducted using Sievers 5310C laboratory TOC analyzer by General Electric (USA). The system measures the amount of carbon dioxide produced upon oxidation through a percolating specific membrane by difference of conductivity [25].

2.2.5. Solid phase extraction

Solid phase extraction (SPE) was carried out on a Supelco Visiprep SPE cell. SPE cartridges used were Supelclean LC-18 SPE tube with 500 mg bed weight and 6 mL volume. All extractions were done at a rate of 50 drops/min as recommended by the supplier. Prior to sample extraction, SPE cartridges were conditioned with 5 mL of ACN at a flow rate of 50 drops/min. The% recovery was tested by passing 1 mL of NAP solution (79 μM) with the same flow rate through the cartridge and extracted with 10 mL ACN. The extract was then purged with N_2 gas until all solvent has evaporated. The residues were dissolved in 1 mL of MeOH and injected into the HPLC to measure NAP concentration using the calibration curve. The% recovery was always found to be greater than 98%. As for the collected samples, the same procedure was followed and aliquots were injected either into the HPLC/MS or the GC/MS, especially for by-products identification.

2.3. Experimental setup

All reagents were prepared as stock solutions from which dilutions were made. The stock solutions were prepared as follows: 20 mg of NAP sodium (79 μM) were dissolved in 1 L of DI water and left to stir over night. The NAP stock solution was filtered using a 0.45 μm PTFE filter and kept at 4 °C for a period no longer than 1 week. PS stock solution was prepared by dissolving 2.3810 g of sodium PS in 100 mL DI water so as to give a 0.100 M stock solution. As for the stock of phosphate buffer (PB) solution, a 0.200 M solution of pH 7.50 was prepared by dissolving 3.1698 g and 3.343 g of NaH_2PO_4 and Na_2HPO_4, respectively in 100 mL DI water. KI solution used for PS complexation was prepared by dissolving 25 g of KI in 250 mL of carbonated DI water. PS, PB and KI stock solutions were prepared on a daily basis.

For the work done on the HE, 10 L were collected at 6:00 a.m. from the final sewage hole of the hospital. The sampling point is located before the waste water is introduced into the Beirut municipal sewage system. The HE was collected in a PTFE bottle and immediately went through several steps of pre-treatment. Gravity filtration using cotton was done in order to remove any large solid waste in the water. Suction filtration through a 0.45 μm filter was performed to remove fine particles. Ultra-centrifugation for 30 min at 15,000 rpm (Sorvall Discovery 100SE Ultracentrifuge, Hitachi) was performed to remove any particles less than 0.45 μm in size which remained suspended in solution. The clear water remaining was then decanted and stored in an amber bottle at 4 °C for a maximum period of a week. A new 10 L water sample was collected again at the same time when needed and treated similar to what has been described above.

All reactions were performed in 20 mL Pyrex vials, and predetermined volumes of each stock solution were added to reach the final desired concentrations e.g. $[NAP]_0$ = 50 μM, $[PS]_0$ = 1.0 mM and [PB] = 50 μM. Vials were placed in a temperature controlled (±1 °C) water bath with the required temperature preset (range 40–70 °C). At the desired times, a vial was removed from the water bath, and the reaction was thermally quenched by cooling the vial to 4 °C in an ice bath [22,23]. Experiments were performed over a period of 2 h during which the pH was measured at the start and end of each reaction using a pH/Ion meter (Thermo Orion, USA) equipped with an ultra-combination pH electrode (Ross). Control experiments were performed in the absence of PS, and all experiments were done in triplicate.

3. Results and discussion

3.1. Temperature effect

As it can be seen from Fig. 1a, the degradation rate of NAP solution is temperature dependent. All reactions undertaken at different temperatures (40, 50, 60 and 70 °C) fit well the pseudo first-order kinetics with a correlation coefficient R^2 always greater than 0.9800. The corresponding observed degradation rate constants (k_{obs}) calculated from the slope of the plots of $\mathrm{Ln}([NAP]/[NAP]_0)$ vs Time ranged between 9.90×10^{-4} mM min^{-1} for the lowest temperature (40 °C) and 1.29×10^{-1} mM min^{-1} for the highest temperature (70 °C) as summarized in Table 1. Fig. 1b shows the Arrhenius plot of NAP degradation at different temperatures. Since $\mathrm{Ln}(k_{obs})$ decreases linearly when plotted against $1/T$, the systems can be fitted into the Arrhenius model (Eq. (6)) with good linearity showing a correlation coefficient of about R^2 = 0.9848:

$$\mathrm{Ln}(k_{obs}) = \mathrm{Ln}(A) - \frac{E_A}{RT} \quad (6)$$

where A is the pre-exponential factor found from the intercept of the Arrhenius plot, E_A is the activation energy (J mol^{-1}), T is the temperature (K) and R the universal gas constant (R = 8.314 J mol^{-1} K^{-1}). Using this model, the activation energy (E_A) was found equal to 155.03 (±26.4) kJ mol^{-1} (Table 2). This value is less than the one obtained for ibuprofen (IBU) (168.0 (±9.5) kJ mol^{-1}) [23] and greater than that of bisoprolol (BIS) β-blocker (119.8 (±10.8) kJ mol^{-1}) [22], making IBU the most recalcitrant pharmaceutical followed by NAP, BIS and antipyrine [32]. The latter's having the lowest activation energy of 16.55 kJ mol^{-1} can be explained by the presence of a 5-member ring pyrazole cycle very vulnerable to oxidation by hydrogen abstraction through $HO^{\cdot}$ and/or electron transfer (ET) through $SO_4^{\cdot-}$. As for the other compounds, one can notice that molecules identified with more ether functions showed the lowest E_A. e.g. BIS. This can be explained by the presence of oxygen atoms (ether groups) vulnerable to oxidative radicals (abstraction of nonbonding electrons from oxygen atoms by $SO_4^{\cdot-}$) more than molecules of comparable structure exempted from ether groups [33]. Finally, it is important to mention that the calculated activation energies of selected probes in TAP systems could be affected by the activation energy of PS upon conversion to sulfate radicals. However, at 60 °C for example, and over a short period of time e.g. 60 min, none of the systems investigated (e.g. probe/PS/PB, PS/PB and PS/H_2O) influenced PS consumption, and therefore PS activation energy [23, Fig. 4S]. Accordingly, one can assume non-significant effect of PS activation energy on the calculated NAP activation energy in the present case. Fig. 2 summarizes the maximum and average values of the RSEs obtained for all oxidation reactions undertaken at different temperatures e.g. 40–70 °C. The RSE is the number of NAP moles degraded over the number of PS moles consumed during a specific time interval $\left[\mathrm{RSE} = \frac{\Delta n(\mathrm{NAP})}{\Delta n(\mathrm{PS})}\right]$. As it can be noticed, the calculated RSEs (maxima and averages) follow the same trend in terms of reaction temperature. For example, the maximum RSEs are noticed at 70 °C (RSE = 68%) and 50 °C (48%), while the minimum RSEs obtained are for reactions occurring at 40 °C (RSE = 7.5%) and 60 °C (24%). Compared to previous work done on different pharmaceuticals under similar conditions, NAP showed lesser RSE values at 60 °C. For example the calculated RSEs for BIS and IBU after 1 h of reaction were about 65% and 70%, respectively [22,23]. This observation has important input on the interpretation of the kinetics law and the role of dissolved species involved in the oxidation mechanisms. As mentioned in Table 2, k_{obs} of NAP is the smallest one ($k_{obs} = 1.64 \times 10^{-2}$ min^{-1}) followed by IBU ($k_{obs} = 2.49 \times 10^{-2}$ min^{-1}) and BIS ($k_{obs} = 8.47 \times 10^{-2}$ min^{-1}) under pseudo-first order

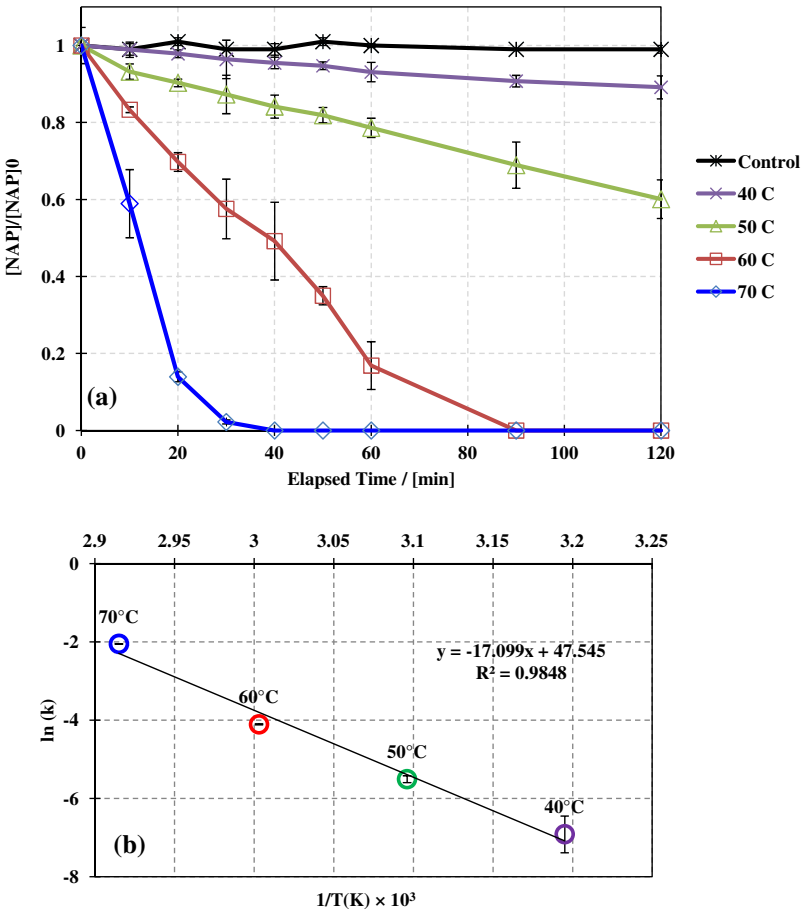

Fig. 1. (a) Temperature effect on the degradation of NAP via thermally activated persulfate. Solid lines are not fitting functions; they are used in order to connect data. Experimental conditions: $[NAP]_0$ = 50 μM, [PS] = 1.0 mM, PB at pH 7.50. Error bars representing standard deviation are calculated at 95% confidence level. (b) Arrhenius plot for the temperature effect experiments. The control experiment was done at 70 °C in PS-free solution. Uncertainties were calculated from standard deviation on the slope determined after using the LINEST function of Microsoft excel.

Table 1
k_{obs} calculated at different temperatures.

Temperature (°C)	k_{obs} (mM min^{-1})	R^2
40	9.90×10^{-4}	0.9844
50	4.05×10^{-3}	0.9874
60	2.69×10^{-2}	0.9837
70	1.29×10^{-1}	0.9893

kinetics model. Accordingly, it is not surprising to notice lesser RSEs for NAP at 60 °C because its chemical structure is more susceptible to $SO_4^{\cdot-}$ than $HO^{\cdot}$. BIS and IBU showed almost equal affinity (45–55%) toward $SO_4^{\cdot-}$ and $HO^{\cdot}$ as well [22,23] in contrast to NAP whose affinity to $SO_4^{\cdot-}$ was much stronger (90% for $SO_4^{\cdot-}$ against only 10% for $HO^{\cdot}$ as per quenching experiments data (Section 3.3). Therefore, more PS is consumed for lesser NAP degradation, dropping thereby RSE values from 65% to 70% to less than 30%. Therefore, RSE values with respect to PS consumed cannot be used as a valid indicator to evaluate TAP effectiveness, especially with pharmaceutical probes of different structures and properties. Details on the most active oxidant toward NAP are provided in Section 3.3.

3.2. Persulfate dosage and effect on mineralization

Previous studies showed that although some pharmaceutical active ingredients undergo thermal persulfate oxidation, acceptable mineralization yields are not reached unless higher concentrations of persulfate are used [23,25]. In this work, a comparative study was done so as to demonstrate complete mineralization of NAP in two different matrices. A control measurement of the TOC content of a starting NAP solution of 50 μM matched well with the theoretical TOC value of NAP molecule e.g. 8.45 mg L^{-1} vs 8.40 mg L^{-1} as for sulfamethoxazole previously investigated [25]. Experiments were undertaken on NAP dissolved in (i) UP water and (ii) HE matrix at 70 °C. The results showed that any PS:NAP molar ratio above (20:1) was enough to fully degrade NAP, however at different contact times. For example, NAP totally disappeared after 60, 30, 20, 10 and 10 min of reaction for PS concentration of about 1.0, 2.5, 5.0, 7.5 and 10.0 mM, respectively (Fig. 3a). Although full NAP degradation was reached, this was not sufficient to reach significant NAP mineralization as per TOC data (Fig. 3b). Accordingly, PS concentration was increased in increments from 1.0 mM to 10 mM yielding an upper limit molar ratio PS:NAP of about 200:1. As it can be noticed from Fig. 3b, at 1.0 mM PS, no mineralization was observed. However, a minimum acceptable molar ratio PS:NAP of about (50:1) was needed in order to exhibit little mineralization that does not exceed 10%. As the concentration of PS increases from 2.5 to 7.5 mM, one can notice a linear mineralization trend with correlation coefficients R^2 of about 0.9911 and 0.9964 for UP water and HE systems, respectively. However, the linear dynamic range in the case of the HE system (2.5–10.0 mM) is greater than the one noticed for UP water system (2.5–7.5 mM). Furthermore, mineralization of NAP in UP water is more significant e.g. 42% and 90% against 30% and 65%

Table 2
Comparison between the chemical and physical properties of NAP and other pharmaceuticals from previous work, as well as the experimental observed degradation rates (k_{obs}) and the calculated activation energies (E_A).

	Bisoprolol	Ibuprofen	Naproxen	Antipyrine
Medicinal property	β-blocker Hypertension	Non-steroidal Anti-inflammatory	Non-steroidal Anti-inflammatory	Analgesic and Antipyretic
Chemical formula	$C_{18}H_{31}NO_4$	$C_{13}H_{18}O_2$	$C_{14}H_{14}O_3$	$C_{11}H_{12}N_2O$
Molecular weight (g mol^{-1})	325.44	206.29	230.259	188.226
Chemical structure	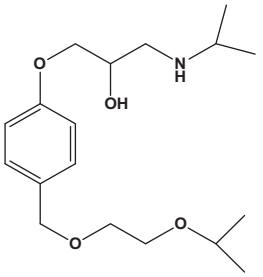	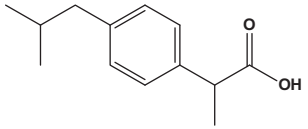	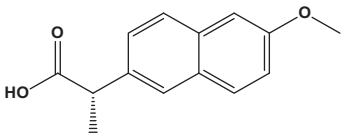	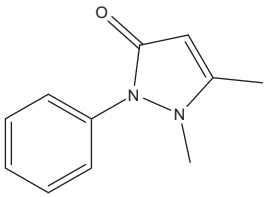
Solubility (mg L^{-1})	2240	21	15.9	51,900
p*K*a	9.5	4.91	4.15	1.4
Density (g mL^{-1})	1.033	1.029	1.197	1.190
Melting point (°C)	100	75–78	152–155	113
k_{obs} at 60 °C ($\times 10^{-2}$ min^{-1})	8.47[a]	2.49[b]	1.64	54.5[c]
E_A (kJ mol^{-1})	119.8 (±10.8)	168.0 (±9.5)	155.0 (±26.4)	16.55

[a] Ghauch et al. [22].
[b] Ghauch et al. [23].
[c] Calculated from k_{obs} reported in s^{-1}; Tan et al. [32].

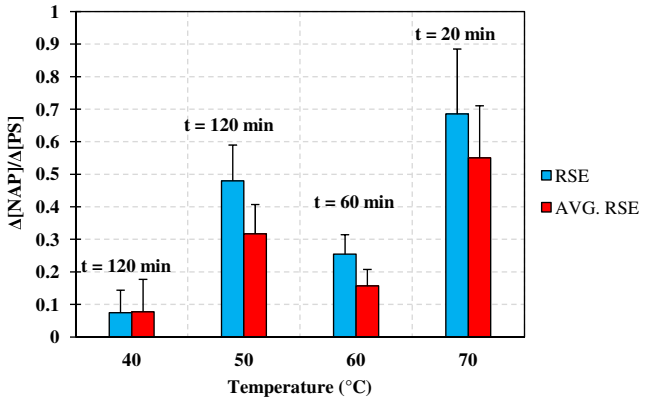

Fig. 2. Maximum and average RSE values noticed at different reaction times under different temperatures. The calculated RSEs are from data collected in Fig. 1. Error bars representing standard deviation are calculated at 95% confidence level.

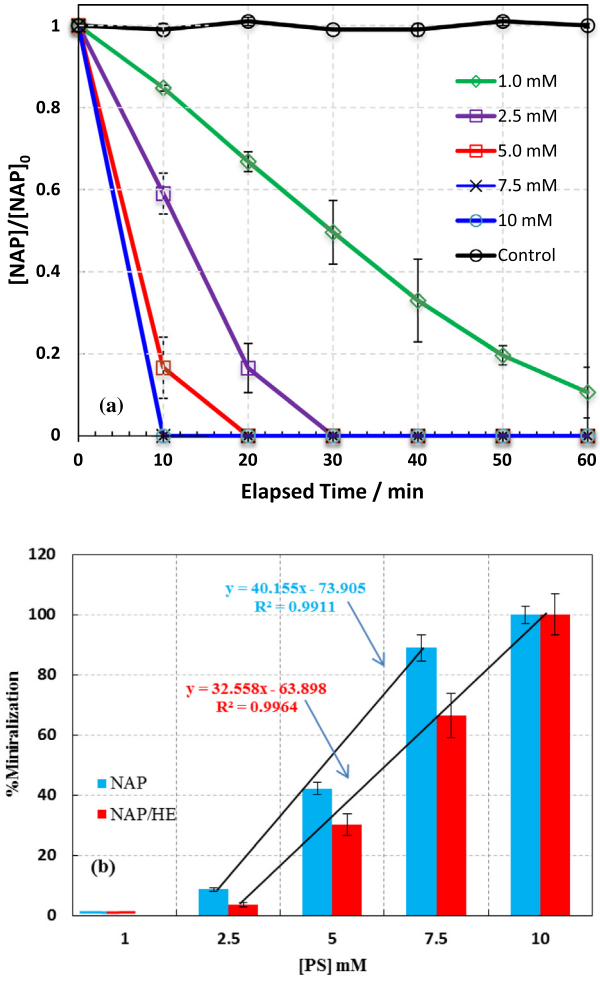

Fig. 3. (a) Time course degradation of NAP as a function of [PS] increasing additive at 60 °C. Curves corresponding to 7.5 and 10.0 mM are overlapping. (b) % mineralization of NAP in ultra-pure water and in hospital effluents (HE) based on TOC measurements. The inline curves correspond to the linear mineralization trend obtained for a specific range of PS concentration: 2.5–7.5 mM for UP water and 2.5–10.0 mM in HE matrix. Experimental conditions are $[NAP]_0$ = 50 μM, [PB] = 50 μM, pH 7.50, T = 70 °C.

for UP water and HE, at 5.0 and 7.5 mM PS, respectively. This difference in the mineralization extent could be attributed to the HE's content. Although in the current study the composition of this particular HE was not determined, it should have similar composition as the hybrid wastewater generated by any similar medical center. Such an effluent includes at the same time domestic, industrial and effluents of care and medical research. The latter are known to contain pathogenic microorganisms, anti-tumor agents, antibiotics, iodinated contrast media and organohalogen compounds as the AOX (adsorbable organically bound halogens) [34–36]. Such species might quench $SO_4^{\cdot-}$ and $HO^{\cdot}$ minimizing therefore to a certain extent the reaction efficacy and % RSE of the reaction. Fig. 3b shows also that above a critical PS concentration e.g. >10 mM, the matrix effect becomes negligible and full mineralization is reached as well even in HE matrix. Based on the corresponding linearity response curve (Fig. 3b), one can predict that full NAP mineralization in UP water matrix occurred at [PS] = 8.0 mM (see inline curves). It is worth noting that oxic solutions favor more organic contaminants' mineralization in activated PS/H_2O systems as has been recently demonstrated in PS chemically activated systems. Dissolved oxygen is an important parameter to sustain and improve PS-based AOPs [25].

The powerful oxidants $SO_4^{\cdot-}$ and $HO^{\cdot}$ thermally generated in solution are responsible for this high mineralization yield. However, in order to check the contribution of each of them to the oxidation process, experiments were conducted in the presence of alcohols having different affinities towards generated radicals.

3.3. Investigations into predominant oxidants in PS/NAP systems ($SO_4^{\cdot-}$ *vs* $HO^{\cdot}$)

Previous studies demonstrated that PS not only produces $SO_4^{\cdot-}$ reacting through ET mechanism once activated [37], but it also generates, upon reaction with water (Eq. (7)), the highly reactive but non-selective $HO^{\cdot}$ oxidants [30,37–39]. In 1977, Neta et al. [40] demonstrated that oxidation of organic molecules via $SO_4^{\cdot-}$ is more specific to ET. However in the case of $HO^{\cdot}$, the reaction taking place is occurring through hydrogen abstraction. Accordingly, in order to identify the main species responsible for the removal of organic carbons in the studied systems, oxidation experiments were done using excess of ethanol (EtOH) and tert-butyl alcohol (TBA) as radicals' scavengers. EtOH scavenger is responsible for the removal of both $SO_4^{\cdot-}$ and $HO^{\cdot}$ radicals from the system (Eqs. (8) and (9)). Whereas TBA scavenger is more selective by reacting first with $HO^{\cdot}$ as it can be noticed from the difference in the reaction rates provided by Eqs. (10) and (11) ($HO^{\cdot}$ is almost 1000 times more reactive than $SO_4^{\cdot-}$ toward TBA) [23,37,39,40]. Three different systems were tested: System 1 (Fig. 4a) was a scavenger free system (control): scavenger/PS/NAP (0/100/1); System 2 (Fig. 4b) was the $SO_4^{\cdot-}$ and $HO^{\cdot}$ scavenging system: EtOH/PS/NAP (40,000/100/1) and system 3 (Fig. 4c) was the $HO^{\cdot}$ scavenging system: TBA/PS/NAP (40,000/100/1). In all scavenged systems, the concentration of the scavenger was set to be 400 times greater than that of PS in order to secure significant quenching yield compared to that of NAP.

$$SO_4^{\cdot-} + H_2O^{\cdot} \rightarrow HO^{\cdot} + HSO_4^- \quad (7)$$

$$EtOH + HO^{\cdot} \sim 1.2\text{–}2.8 \times 10^9\ M^{-1}\ s^{-1} \quad (8)$$

$$EtOH + SO_4^{\cdot-} \sim 1.6\text{–}7.7 \times 10^7\ M^{-1}\ s^{-1} \quad (9)$$

$$TBA + HO^{\cdot} \sim 3.8\text{–}7.6 \times 10^8\ M^{-1}\ s^{-1} \quad (10)$$

$$TBA + SO_4^{\cdot-} \sim 4.0\text{–}9.1 \times 10^5\ M^{-1}\ s^{-1} \quad (11)$$

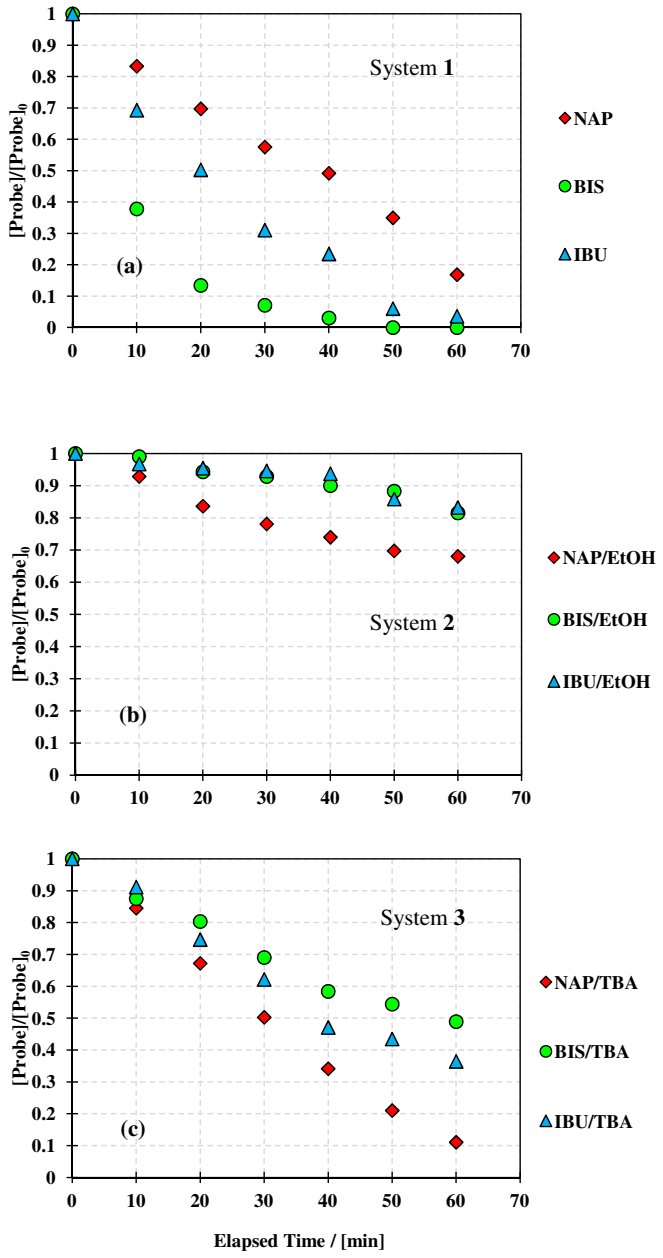

Fig. 4. (a) Scavenger free degradation of NAP, BIS[1] and IBU[2]. (b) Effect of EtOH radical scavenger on the removal of NAP, BIS[1] and IBU[2]. (c) Effect of TBA radical scavenger on the removal of NAP, BIS[1] and IBU[2]. Ratio of Scavenger:PS:Probe was 40,000:100:1 in all experiments. Experimental conditions: $T = 60$ °C, $[NAP]_0 = 50$ μM, $[BIS]_0 = 50$ μM, $[IBU]_0 = 23$ μM, $[PS] = 1.0$ mM, PB at pH 7.50. [1]Ghauch et al. [22]; [2]Ghauch et al. [23].

Fig. 4b shows clearly that when both radials are scavenged (System 2), NAP degradation is less significant with respect to the scavenger free system e.g. 32% vs 82% after 60 min for the scavenged and non-scavenged systems, respectively (Fig. 4a). Nevertheless, when TBA is used, only $SO_4^{\cdot-}$ species remained in solution and achieved 90% NAP degradation at 60 min of reaction (Fig. 4c) to finally reach full degradation after 90 min of reaction (data not shown). This was not the case for BIS [22] and IBU [23] molecules for which both $SO_4^{\cdot-}$ and $HO^{\cdot}$ contributed an average of 42% and 58%, respectively, to the oxidation reactions (Fig. 4c). In contrary to the previous results on BIS and IBU, the present study on NAP degradation suggests that even with the noticeable help of $HO^{\cdot}$, $SO_4^{\cdot-}$ is the most significant radical responsible for NAP removal. For example, in the absence of any $SO_4^{\cdot-}$ quencher, NAP was the most recalcitrant pharmaceutical followed by IBU and BIS (Fig. 4a). However, once $HO^{\cdot}$ radicals were quenched by TBA (Fig. 4c), the degradation trend was reversed, with BIS being the more recalcitrant pharmaceutical followed by IBU and NAP. Accordingly, this behavior towards the reactive oxidant in the medium can be attributed to the difference in the molecular structures and functional groups of NAP, IBU and BIS, as can be seen in Table 2. For example, compared to BIS and IBU, NAP structure shows a more electron-rich environment e.g. presence of a naphthalene moiety, making it more susceptible to oxidation via ET reactions. However, BIS and IBU are less electron-rich entities and present abundance in hydrogen atoms (four CH_3 groups in BIS and three CH_3 groups in IBU vs only one CH_3 group in NAP) that can undergo quickly hydrogen abstraction via $HO^{\cdot}$. This corroborates findings of Klefah et al. [41] who demonstrated that the CH_3 group on NAP molecule acts as a proton donor, which, in its turn, enhances NAP degradation through decarboxylation.

Furthermore, a calculation of the % change in k_{obs} ($\Delta k_{obs} = ((k_{obs(\text{with quencher})}/k_{obs(\text{quencher-free})}) - 1) \times 100$) (Table 3) showed a decrease by −75.1% for NAP upon quenching with EtOH while an increase by +35.8% was noticed with TBA quencher compared to quencher-free NAP solution. This means that NAP degradation was positively affected by $HO^{\cdot}$ quenchers through TBA additive in contrast to BIS and IBU that showed a decrease in their degradation rate constant Δk_{obs} of about −85.8% and −66.8%, respectively. The improvement of NAP degradation kinetics reported in the presence of TBA might be related to the high NAP- $SO_4^{\cdot-}$ reaction rate greater than that of TBA-$SO_4^{\cdot-}$ reaction in the absence of radical–radical quenching reactions (Eq. (12)). On the other hand, Table 3 showed also that in all radical quenching systems (EtOH additives) Δk_{obs} for NAP was the least affected value with only −75.1% decrease compared to −95.2% and −96.2% for IBU and BIS, respectively. This can be considered as an additional indicator that NAP molecule is much more sensitive to $SO_4^{\cdot-}$ that are more selective toward electron-rich moieties and can be applied to NAP molecules dissolved in complex matrices:

$$SO_4^{\cdot-} + HO^{\cdot} \rightarrow HSO_5^- \quad (12)$$

Table 3
Comparison of NAP kinetics parameters as a function of alcohol additives (scavengers) and ion additives.

Scavengers (mole ratios) (40,000/100/1)	$k_{obs} \times 10^{-2}$ (min^{-1})[a]	$t_{1/2}$[b] (min)	R^2	% Δk_{obs}
Additive free	2.65 ± 0.09	24.07	0.9837	0
EtOH/PS/NAP	0.66 ± 0.03	105.0	0.9628	−75.1
EtOH/PS/BIS[c]	0.32 ± 0.03	216.1	0.9059	−96.2
EtOH/PS/IBU[d]	0.26 ± 0.03	267.1	0.8380	−95.2
TBA/PS/NAP	3.60 ± 0.03	19.3	0.9939	+35.8
TBA/PS/BIS[d]	1.20 ± 0.04	57.8	0.9836	−85.8
TBA/PS/IBU[e]	1.82 ± 0.03	38.2	0.9757	−66.8
Ion additives (mg L^{-1})	$k_{obs} \times 10^{-2}$ (min^{-1})[a]	$t_{1/2}$[b] (min)	R^2	% Δk_{obs}
$CaCl_2$ (5.0)[e]	2.16 ± 0.06	37.27	0.9918	−18.49
$CaSO_4$ (50)	4.90 ± 0.66	16.35	0.9452	+84.9
$NaHCO_3$ (160)	4.29 ± 0.27	24.24	0.9816	+61.9
$MgNO_3$ (5.0)	6.74 ± 0.56	7.66	0.8289	+154.3
Drinking water	4.60 ± 0.33	18.94	0.9775	+73.6

[a] k_{obs} are obtained from the slopes of the plots of $Ln([NAP]/[NAP]_0)$ vs time. Uncertainties were calculated from standard deviation on the slope determined after using the LINEST function of Microsoft excel.
[b] Calculated from the pseudo-first order equation where $t_{1/2} = Ln2/k_{obs}$.
[c] Data are from Ref. [20] where Δk_{obs} is calculated with respect to the k_{obs} of scavenger-free solution.
[d] Data are from Ref. [21] where Δk_{obs} is calculated with respect to the k_{obs} of scavenger-free solution.
[e] Concentration of additives (mg L^{-1}).

3.4. Matrix effect

3.4.1. Case of inorganic additives

In real-life application of water treatment using TAP systems, several factors may interfere with the reaction rates and RSEs. In addition to humic acids [42,43], dissolved inorganic species in water are one of those factors. As a method of studying the effect of these inorganic additives on NAP degradation in water, experiments were performed with the addition of $NaHCO_3$, $CaSO_4$, $CaCl_2$ and $Mg(NO_3)_2$ at concentrations mimicking those of natural/spring waters e.g. $[Na^+] = [HCO_3^-] = 160$; $[Ca^{2+}] = [SO_4^{2-}] = 50$; $[Cl^-] = 5.0$ and $[Mg^{2+}] = [NO_3^-] = 5.0$ mg L^{-1}. The chosen salts do not have common cations since it was previously demonstrated that cations are not supposed to influence sulfate radical chemistry at such concentration [22]. Each inorganic additive was added separately to NAP:PS (1:20) systems and the reactor was heated to 60 °C for oxidation reactions. The k_{obs} of these reactions were calculated at appropriate reaction times (before complete NAP vanishing) with respect to pseudo-first order kinetics and reported in Table 3. As it can be noticed, all additives showed an increase in k_{obs} values with respect to the additive-free solution (Fig. 5, dash line), except for $CaCl_2$.

The addition of $CaCl_2$ showed a decrease in Δk_{obs} value of about −18.49%. In fact, chlorides in solutions are the precursors of chlorine and dichlorine radicals e.g. $Cl^{\cdot}$ and $Cl_2^{\cdot-}$ responsible for side quenching reactions of $SO_4^{\cdot-}$ (Eqs. (13) and (14)). Therefore, less $SO_4^{\cdot-}$ are available for NAP oxidation:

$$SO_4^{\cdot-} + Cl^- \rightarrow Cl^{\cdot} + SO_4^{2-} \quad k = 3.1 \times 10^8 \text{ L mol}^{-1} \text{ s}^{-1} \text{ at pH 6.8} \tag{13}$$

$$Cl^{\cdot} + Cl^- \rightarrow Cl_2^{\cdot-} \quad k = 2.1 \times 10^{10} \text{ L mol}^{-1} \text{ s}^{-1} \tag{14}$$

Although $Cl^{\cdot}$ and $Cl_2^{\cdot-}$ are known by their oxidative properties toward organic compounds, in a slightly basic medium as it is the case here (7.50 < pH < 7.86), $Cl^{\cdot}$ is more reactive toward hydroxyl species than organic compounds (Eq. (15)) [44,45]. This most probably can explain the slight decrease in the k_{obs} of NAP compared to a slight increase as previously reported for BIS [22] where the pH was relatively acidic (6.70 < pH < 7.00), favoring therefore the dissociation of $ClOH^{\cdot-}$ into $Cl^{\cdot}$ (Eq. (16)). In addition, $Cl^{\cdot}$ might also be quenched by water, however, at a much slower rate compared to that of hydroxyl species (Eq. (17)) [45,46]:

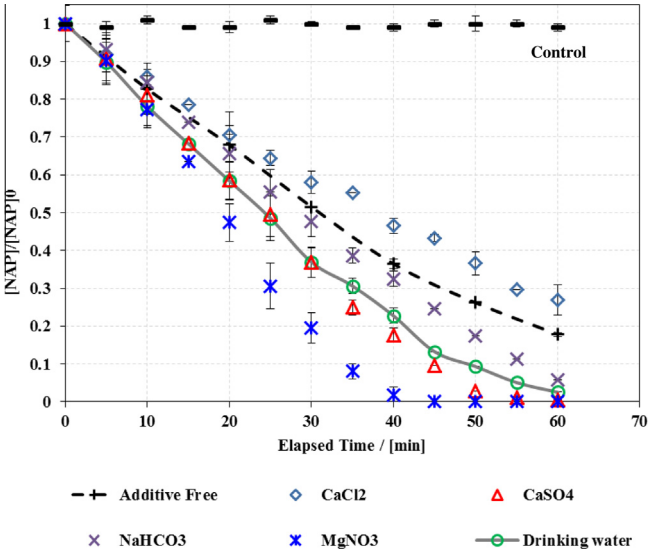

Fig. 5. Effect of inorganic additives on the removal of NAP. The control experiment was done in PS-free solution. Experimental conditions: $[NAP]_0 = 50$ μM, [PS] = 1.0 mM, $T = 60$ °C, PB at pH 7.50.

$$Cl^{\cdot} + OH^- \rightarrow ClOH^{\cdot-} \quad k = 1.8 \times 10^{10} \text{ L mol}^{-1} \text{ s}^{-1} \tag{15}$$

$$HOCl^{\cdot-} + H^+ \rightarrow Cl^{\cdot} + H_2O \tag{16}$$

$$Cl^{\cdot} + H_2O \rightarrow ClOH^- + H^+ \quad k = 1.6 \times 10^5 \text{ s}^{-1} \tag{17}$$

On the other hand, the greater improvement among all additives was noticed with $MgNO_3$ exhibiting a Δk_{obs} value of about +154.3%. This is not surprising since Δk_{obs} improvement has already been noticed in a previous work under similar conditions such as BIS removal, whose degradation was shown dependent on $SO_4^{\cdot-}$ and $HO^{\cdot}$ equally [20]. In fact $SO_4^{\cdot-}$ can produce in the medium $NO_3^{\cdot}$ (Eq. (18)) having a high redox potential ($E_{1/2} = 2.50$ V) for more NAP oxidation [46,47]:

$$SO_4^{\cdot-} + NO_3^- \rightarrow SO_4^{2-} + NO_3^{\cdot} \quad k = 2.1 \times 10^6 \text{ L mol}^{-1} \text{ s}^{-1} \text{ at pH 7–8} \tag{18}$$

In the case of $CaSO_4$ additive, a lesser improvement was noticed with a Δk_{obs} value of about +84.9%. In this case, $SO_4^{\cdot-}$ might be scavenged by similar radicals regenerating in the medium PS species that contribute again to oxidation reactions upon heating (Eq. (18)). This process could therefore sustain high NAP oxidation yield:

$$SO_4^{\cdot-} + SO_4^{\cdot-} \leftrightarrow S_2O_8^{2-} \tag{19}$$

Finally, the least improvement was noticed in $NaHCO_3$-spiked NAP solution (Δk_{obs} = +61.9%). Basically, HCO_3^- species react with $SO_4^{\cdot-}$ to produce $CO_3^{\cdot-}$ radicals (Eq. (20)). Those have also positive redox potential ($E_{1/2}^{red}$ = 1.50 V) comparable to that of $NO_3^{\cdot}$ ($E_{1/2}^{red}$ = 2.50 V), $SO_4^{\cdot-}$ $E_{1/2}^{red}$ = 2.43 V) and $Cl_2^{\cdot-}$ ($E_{1/2}^{red}$ = 2.09 V) [46–48]. Accordingly, an enhancement in k_{obs} with regard to bicarbonate-free solution is not surprising. In fact, the selected probe e.g. NAP has good affinity toward $CO_3^{\cdot-}$ in contrast to BIS that showed a decrease in its k_{obs} in bicarbonate-spiked solution [22]. BIS degradation, in contrast to NAP degradation, showed more implication of $HO^{\cdot}$ more quenched by HCO_3^- species (Eq. (21)) [48]:

$$SO_4^{\cdot-} + HCO_3^- \rightarrow SO_4^{2-} + CO_3^{\cdot-} + H^+ \quad k = 8.5 \times 10^6 \text{ L mol}^{-1} \text{ s}^{-1} \tag{20}$$

$$HO^{\cdot} + HCO_3^- \rightarrow CO_3^{\cdot-} + H_2O \quad k = 1.6 \times 10^6 \text{ L mol}^{-1} \text{ s}^{-1} \tag{21}$$

3.4.2. Case of drinking water and hospital effluent (HE)

TAP process was also applied to a NAP-spiked commercial mineral drinking water having almost a similar composition range in inorganic species as previously reported (Section 3.4.1). The mineral drinking water is assumed to not contain any organic species except the spiked NAP solution. Its composition as per its label denominates the following ions given in mg L^{-1}: $[Ca^{2+}] = 33$; $[Mg^{2+}] = 16$; $[SO_4^{2-}] = 12$; $[NO_3^-] = 1.5$; $[Cl^-] = 7$ and $[HCO_3^-] = 150$. The results showed complete degradation of NAP after 60 min of reaction time (Fig. 5, solid line) with an improved Δk_{obs} of about +73.6% as per comparison to an additive-free NAP solution (Table 3). Accordingly, little or no quenching reactions occurred during the treatment of this solution. This reduced quenching can be considered as an advantage for TAP application to drinking water supplies slightly charged in dissolved inorganic species.

In order to further explore the potential of TAP systems in degrading organic contaminants regardless of the matrix content, 20 mL sample of processed HE was spiked with 50 μM of NAP. Based on the TOC data of previous experiments (Fig. 3b), 10 mM of PS were added to the spiked HE and treated for 2 h at 70 °C. As can been seen in Fig. 6, the HPLC chromatographic peak of NAP (retention time = 35 min) totally vanished after TAP treatment. In

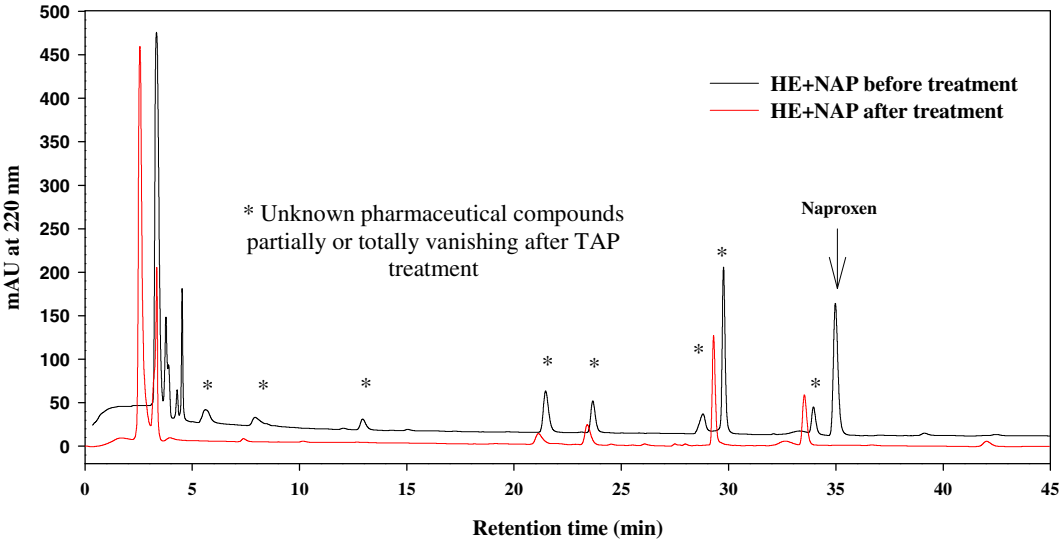

Fig. 6. HPLC/DAD spectrum of hospital effluent spiked with NAP before and after treatment with PS. Experimental conditions: [NAP] = 50 μM; [PS] = 10 mM; T = 70 °C; reaction time = 2 h.

addition, other peaks corresponding to unknown organic compounds (indicated with an "*" on the chromatogram) disappeared partially or totally, demonstrating that TAP can be considered as a universal treatment method to be applied to highly charged effluents like HE.

3.5. Transformation products

Time course profiles for the disappearance of NAP and the appearance/disappearance of its transformation products are shown in Fig. 2S. As it can be noticed, NAP totally disappeared after 40 min of reaction. At the same time, two of its by-products BP**1** and BP**2** reached a maximum of concentration in solution at 20 min of reaction then totally vanished at 50 min. However, a third by-product BP**3** showed an increase in its concentration up to 50 min followed by a significant decline up to 2 h of reaction. Based on this observation, one can deduce that direct and successive oxidation reactions are very plausible so that BP**1** and BP**2** disappeared in favor of BP**3** that is considered the final transformation product before its total degradation at longer reaction time (data not shown). In order to confirm such a hypothesis that allows the elucidation of a degradation mechanism of NAP in TAP systems, HPLC–DAD-FLD–MS and GC/MS analyses were performed, however, in the absence of authentic standards. In HPLC/MS analysis, the atmospheric pressure photo-ionization head did not show any response for NAP and its transformation products, although in the presence of a dopant e.g. acetone, toluene. On the contrary, electrospray ionization (ESI) showed significant response for NAP and its transformation products in positive ionization (PI) mode (Fig. 7 and Table 4) while negative ionization (NI) mode was successful with NAP only (Fig. 3S and Table 1S). Accordingly, PI mode was adopted for the identification of all transformation products. Furthermore, the GC/MS analysis done in electron impact mode, after SPE preparation, showed the MS spectra of NAP and two of its by-products (BP**1** and BP**3**) (Table 2S), thereby confirming the identity of two transformation products previously analyzed by HPLC/MS.

3.5.1. UV/vis and fluorescence analyses

Fig. 7 shows the TIC of NAP solution during TAP process at 20 min of reaction. Under the current analytical conditions, NAP was eluted at 7.1 min, BP**1**, BP**2** and BP**3** at 6.4, 7.9 and 10.15 min, respectively. The DAD results showed almost similar UV/vis absorbance spectra for NAP, BP**1** and BP**2** with a very small blue shift (hypsochromic) of about $\Delta\lambda$ = 2 nm (λ_{max} = 232 nm for NAP and 230 nm for BP**1** and BP**2**) that could explain the formation of a lesser conjugated molecule (Inset Fig. 7b). As for BP**3**, a red shift is obvious with two λ_{max} at 242 nm and 310 nm ($\Delta\lambda$ = 10 nm and 35 nm), thereby confirming the formation of a more conjugated electronic system (Inset Fig. 7b). In an oxidative medium and in the presence of dissolved oxygen, the formation of a ketone moiety (C=O group) could take place. This corroborates previous findings [10,49,50] that reported the formation of BP**3** upon photolysis of NAP in oxic solution. On the other hand, BP**1** showed high fluorescence yield ($\lambda_{max\ (em)}$ = 360 nm) compared to NAP ($\lambda_{max\ (em)}$ = 356 nm) while BP**2** is much less fluorescent ($\lambda_{max\ (em)}$ = 355 nm). However, BP**3** did not show any fluorescence at the same excitation wavelength e.g. λ_{ex} = 230 nm. Such an observation can be considered as an advantage transforming the parent fluorescent compound (NAP) to non-fluorescent compound in terms of reduced photosensitivity [49]. However, in the absence of authentic standards, MS analysis was conducted in order to identify all transformation products based on their fragmentation patterns.

3.5.2. HPLC/MS and GC/MS analyses

HPLC/MS spectra of NAP and all its transformation products are listed in Table 4. Under the current analytical conditions, NAP showed two adducts at 253.1 and 275.0 m/z corresponding to $[M+Na]^+$ and $[M+2Na-H]^+$, respectively. It also showed the base peak of the molecular ion $[M+H]^+$ at 231.1 m/z and the decarboxylated fragment $[M\text{-}COOH]^+$ at 185.1 m/z. BP**1** has a base peak molecular ion $[M+H]^+$ at 185.1 m/z corresponding to a decarboxylated NAP molecule (2-methoxy-6-vinylnaphthalene) and a potassium adduct $[M+K]^+$ at 223.1 m/z. BP**2** depicted a base peak molecular ion $[M+H]^+$ at 201.1 m/z and two adducts $[M+Na]^+$ and $[M+K]^+$ at 223.1 and 239.1 m/z, respectively. It also showed a fragment at 185.1 m/z that can be attributed to the loss of an oxygen atom (16 amu) from the oxidized aldehyde NAP derivative (2-(6-methoxynaphthalen-2-yl)acetaldehyde). BP**3** has the same molecular ion $[M+H]^+$ as BP**2**; however, both does not have the same fragmentation pattern and adducts. This fact indicates that BP**2** and BP**3** have different structures (Isomers). For example, only sodium adduct $[M+Na]^+$ is noticed at 223.1 m/z while potassium adduct is absent. Furthermore, non-identified significant fragments e.g. 161.9 and

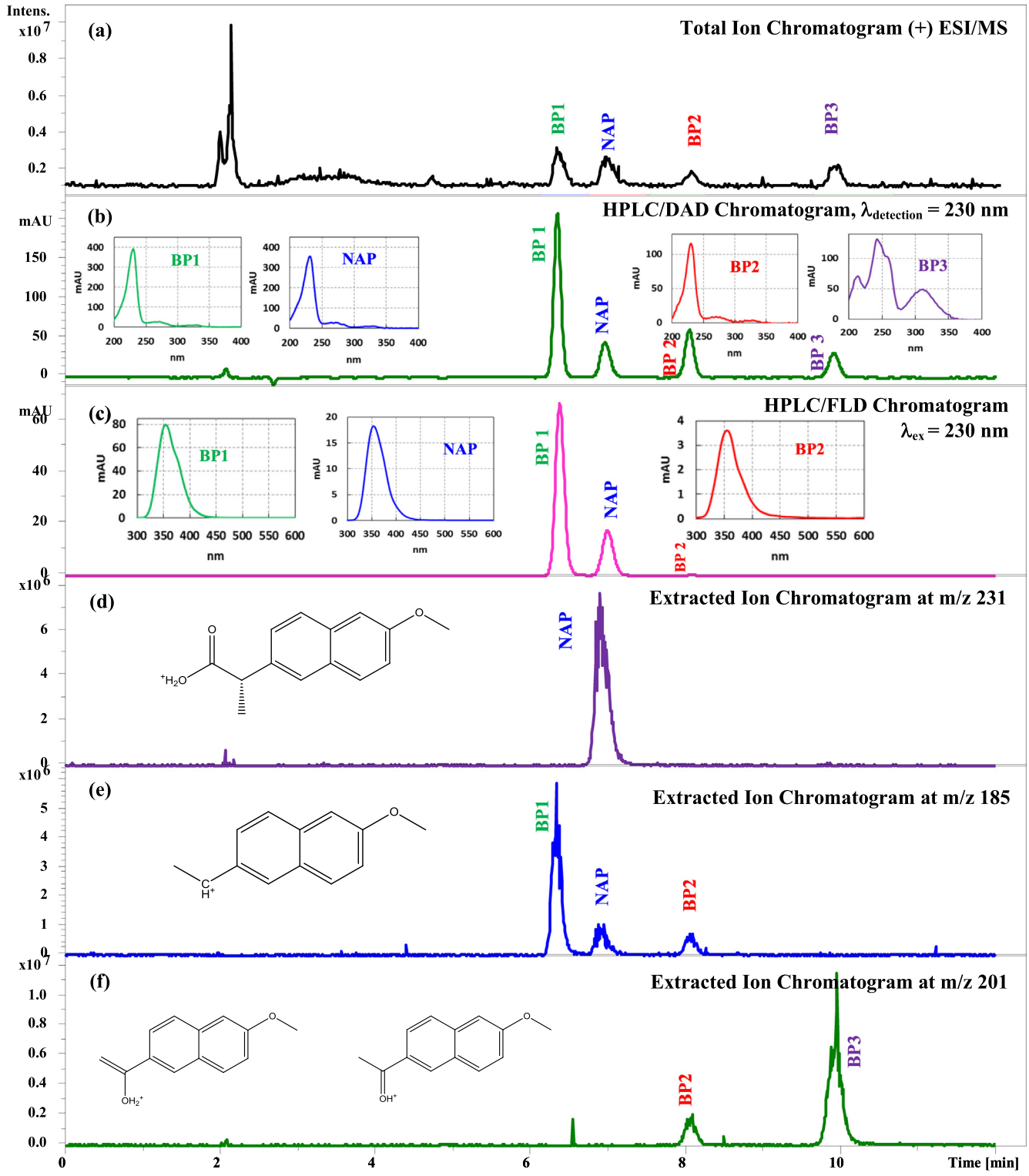

Fig. 7. (+) ESI/MS (a), UV/DAD (b) and UV/FLD (c) chromatograms and the corresponding extracted ion chromatograms (d–f) obtained by HPLC/ESI/MS in positive ionization mode on the NAP solution (100 μM) after 20 min of contact with PS (1.0 mM) at 70 °C in oxic solution at (231 ± 0.5), (185 ± 0.5) and (201 ± 0.5) *m/z* for NAP, BP**1** and BP**2** and BP**3**, respectively. Insets represent the (i) UV/vis absorbance (b) and fluorescence (c) spectra of NAP and its transformation products e.g. BP**1**, BP**2** and BP**3** and (ii) the chemical structures of the proposed positively ionized fragments (d–f).

153.5 *m/z* are present. Those can be attributed to some mass losses followed by molecule rearrangement in the mass analyzer. However, based on the UV/vis analyses shown above, BP**3** should correspond to the ketone isomer providing more electron conjugation to the molecule. Accordingly, BP**2** and BP**3** are the result of oxidation of BP**1** after its decarboxylation.

In order to confirm this hypothesis and further investigate into the transformation products, GC/MS spectra summarized in

Table 4
Proposed name of NAP degradation products and their corresponding analytical properties using GC/MS and HPLC/DAD/MS analyses upon solid phase extraction.

Name	MW	Proposed Structure	Rt (min)	(+)ESI/MS spectrum
Naproxen	230.26	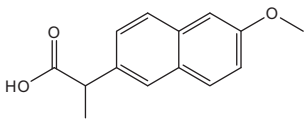	6.72	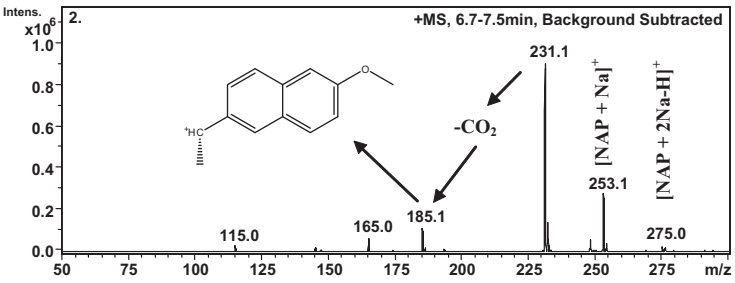
BP**1**	184.23	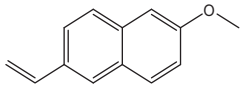	6.22	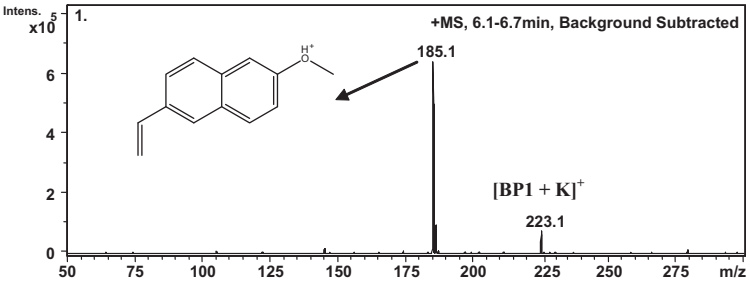
BP**2**	200.23	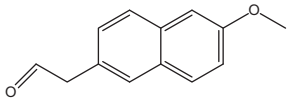	7.77	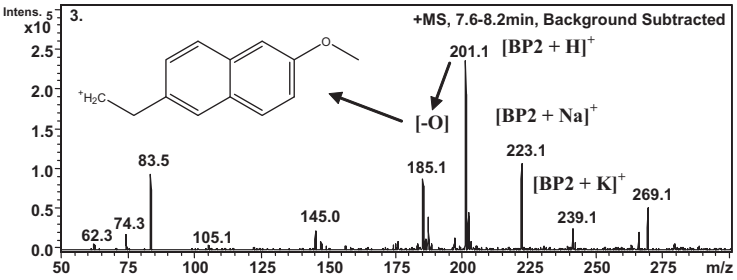
BP**3**	200.23	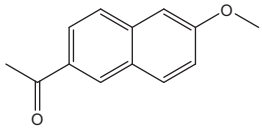	9.45	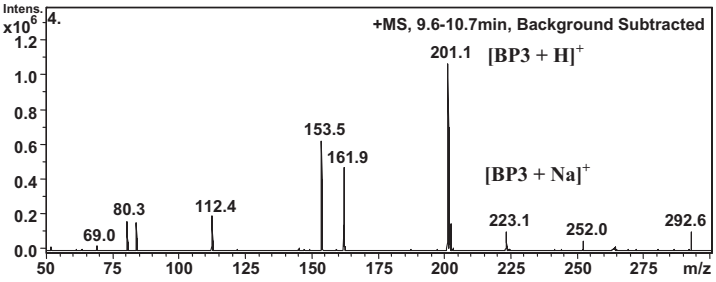

BP**1**: 2-Methoxy-6-vinylnaphthalene, BP**2**: 2-(6-methoxynaphthalen-2-yl)acetaldehyde, BP**3**: 1-(6-methoxynaphthalen-2-yl)ethanone.

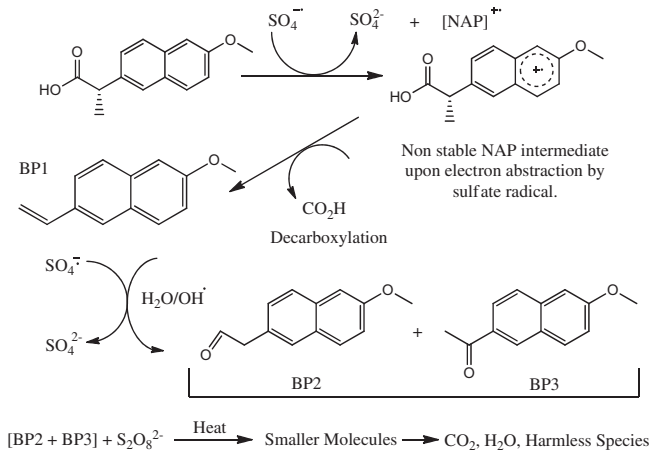

Fig. 8. Proposed degradation scheme of NAP in thermally activated persulfate systems.

Table 2S showed the corresponding molecular ions matching those obtained with the HPLC/MS analysis. For example, NAP showed a molecular ion at 229.9 *m/z*. It also showed a base peak at 214.9 *m/z* and a fragment at 186.8 *m/z* corresponding to the loss of a methyl group (CH_3; 15 amu) and a carboxylic moiety (COOH; 44 amu), respectively [51]. BP**1** showed a base peak molecular ion at 183.9 *m/z* and fragments at 168.9, 140.9 and 114.9 *m/z* corresponding to the losses of CH_3 (15 amu), CH_3CO (43 amu) and (C_4H_5O, 69 amu), respectively. BP**3** showed a molecular ion at 200 *m/z*, a base peak at 184.9 *m/z* and fragments at 156.9 and 114.9 *m/z* corresponding to the loss of the CH_3 (15 amu), CH_3CO (43 amu), and C_4H_4O (69 amu), respectively. BP**2**, however, was not detected by GC/MS. This could be due to the non-stability of the molecule at high temperature.

The obtained NAP by-products (BP**1**, BP**2** and BP**3**) were previously reported in the literature as the most common NAP degradation species regardless of the oxidation method and reaction conditions. For example, Arany et al. [50,51] identified two of those transformation products (BP**1** and BP**3**) upon photolysis of NAP,

whereas Marco-Urrea et al. [38] reported BP**2** as a result of NAP biodegradation. Marotta and co-workers [10] demonstrated the formation of BP**3**, however, after hydroxylation of the decarboxylated NAP during photo-degradation reactions. In this work, no hydroxylated transformation products were identified because the oxidation mechanism mostly relied on $SO_4^{\cdot-}$ instead of $HO^{\cdot}$.

3.5.3. NAP degradation scheme

According to the above investigations and previous data regarding the elucidation of TAP oxidation mechanisms [24,26,52], a scheme of the degradation mechanism of NAP could be proposed as reported in Fig. 8. First, NAP molecule is ionized upon electron abstraction by $SO_4^{\cdot-}$ mostly occurring on the naphthalene ring since its ionization energy (~8.144 eV) [53] is lesser than that of the nonbonding electron pairs on oxygen atoms (⩾10.0 eV) [54] to form NAP radical cation $[NAP]^{\cdot+}$. This is followed by decarboxylation yielding the formation of BP**1**, which undergoes oxidative reaction in the presence of dissolved oxygen. The result of such oxidation is the production of an aldehyde (BP**2**) and a ketone (BP**3**) whereby the latter is more favored as per Fig. 2S kinetics' profile. Finally, BP**3** did not persist in the solution and disappeared as the reaction time is prolonged, and sulfate radicals' precursor remained available in the reactive medium, reaching therefore full mineralization.

4. Conclusion

In this work, TAP system showed once more its effectiveness as a strong oxidant for water treatment technologies. In addition of being able to act under circumneutral pH conditions in clean matrices e.g. DI water, TAP system can also be a great oxidizer regardless of the aqueous matrix in which contaminants are dissolved. The results obtained showed full degradation of NAP in a highly charged non-treated HE. Complete mineralization of pharmaceutical wastes and HEs was obtained under decent conditions according to TOC data. These conditions include cricumneutral pH, short periods of reaction times and economically affordable temperatures e.g. in case solar energy is used. During all experimental work, high RSEs were achieved (e.g. RSE up to 68% after 20 min of reaction at 70 °C). Inorganic additives affected more or less the oxidation process. $MgNO_3$ improved by 154% NAP degradation rate constant while $CaCl_2$ decreased the degradation rate constant by 18.5%. All reactions showed a pseudo first-order degradation kinetics as well as good Arrhenius behavior. The highest achieved k_{obs} was found to be 1.286 mM min^{-1} at 70 °C with an E_A of about 155.0 (±26.4) kJ mol^{-1}. In radical scavenging systems, it was seen that both radical species $HO^{\cdot}$ and $SO_4^{\cdot-}$ played a role in the oxidation process; however, $SO_4^{\cdot-}$ was the most dominant oxidant. This was attributed to the chemical structure of NAP that is rich in non-bonding electrons pairs. This observation was also comforted by the nature of the transformation products where no hydroxylated NAP species were detected. Results showed that after NAP decarboxylation (BP**1**), an aldehyde (BP**2**) and ketone (BP**3**) decarboxylated NAP compounds were identified; BP**3** being the most stable transformation product that totally vanished by the end of the reaction. Future development into potential synergistic effect of solar and chemical activation of PS in aqueous systems along with toxicity assessment will be considered for field application toward direct water reuse [55].

Acknowledgements

This research was funded in part by the University Research Board of the American University of Beirut (Award number 102542) and USAID-Lebanon through The National Academy of Sciences under PEER project 1-084 (Award number 102548). The author is thankful to the personnel of the Kamal Al Shair Central Research Scientific Laboratory (KAS CRSL) for their technical assistance and to Professor David Sedlak from UC-Berkeley for his valuable remarks. The English was improved by Maya Sfeir from the Writing Center at AUB.

Appendix A. Supplementary data

Supplementary data associated with this article can be found, in the online version, at http://dx.doi.org/10.1016/j.cej.2015.05.067.

References

[1] T. Kosjek, E. Heath, A. Krbavcic, Determination of non-steroidal anti-inflammatory drug (NSAIDs) residues in water samples, Environ. Int. 31 (2005) 679–685.
[2] D.W. Kolpin, M. Skopec, M.T. Meyer, E.T. Furlong, S.D. Zaugg, Urban contribution of pharmaceuticals and other organic wastewater contaminants to streams during differing flow conditions, Sci. Total Environ. 328 (2004) 119–130.
[3] J.L. Zhoua, Z.L. Zhang, E. Banks, D. Grover, J.Q. Jiang, Pharmaceutical residues in wastewater treatment works effluents and their impact on receiving river water, J. Hazard. Mater. 166 (2009) 655–661.
[4] M. Isidori, M. Lavorgna, A. Nardelli, A. Parrella, L. Previtera, M. Rubino, Ecotoxicity of naproxen and its phototransformation products, Sci. Total Environ. 348 (2005) 93–101.
[5] S. Ali, J.D. Pimentel, C. Ma, Naproxen-induced liver injury, Hepatob. Pancreat. Dis. 10 (2011) 552–556.
[6] M. Manrique-Moreno, M. Suwalsky, F. Villena, P. Garidel, Effects of the nonsteroidal anti-inflammatory drug naproxen on human erythrocytes and on cell membrane molecular models, Biophys. Chem. 147 (2010) 53–58.
[7] D. Ma, G. Liu, W. Lv, K. Yao, X. Zhang, H. Xiao, Photodegradation of naproxen in water under simulated solar radiation: mechanism, kinetics, and toxicity variation, Environ. Sci. Pollut. Res. Int. 13 (2014) 7797–7804.
[8] F.J. Benitez, J.L. Acero, F.J. Real, G. Roldán, Ozonation of pharmaceutical compounds: rate constants and elimination in various water matrices, Chemosphere 77 (2009) 53–59.
[9] R. Rosal, A. Rodríguez, M.S. Gonzalo, E. García-Calvo, Catalytic ozonation of naproxen and carbamazepine on titanium dioxide, Appl. Catal. B-Environ. 84 (2008) 48–57.
[10] R. Marotta, D. Spasiano, I. Di Somma, R. Andreozzi, Photodegradation of naproxen and its photoproducts in aqueous solution at 254 nm: a kinetic investigation, Water Res. 47 (2013) 373–383.
[11] M. Qurie, M. Khamis, F. Malek, S. Nir, S.A. Bufo, J. Abbadi, L. Scrano, R. Karaman, Stability and removal of naproxen and its metabolite by advanced membrane wastewater treatment plant and micelle-clay complex, Clean Soil, Air, Water 41 (2013) 1–7.
[12] J. Im, J. Heo, L.K. Boateng, N. Her, J.R.V. Flora, J. Yoon, K. Zoh, Y. Yoon, Ultrasonic degradation of acetaminophen and naproxen in the presence of single-walled carbon nanotubes, J. Hazard. Mater. 254–255 (2013) 284–292.
[13] E. Felis, D. Marciocha, J. Surmacz-Gorska, K. Miksch, Photochemical degradation of naproxen in the aquatic environment, Water Sci. Technol. 12 (2007) 281–286.
[14] F.J. Benitez, J.L. Acero, F.J. Real, G. Roldan, F. Casas, Comparison of different chemical oxidation treatments for the removal of selected pharmaceuticals in water matrices, Chem. Eng. J. 168 (2011) 1149–1156.
[15] L. Rein, A. Welch, Toxicity of combinations of naproxen and its photodegradants to toad tadpoles. Society for integrative and comparative biology, College of Charleston, Meeting Abstract, P3.100, 2015.
[16] C. Gadipelly, A. Pérez-González, G.D. Yadav, I. Ortiz, R. Ibáñez, V.K. Rathod, K.V. Marathe, Pharmaceutical industry wastewater: review of the technologies for water treatment and reuse, Ind. Eng. Chem. Res. 29 (2014) 11571–11592.
[17] A. Tsitonaki, B. Petri, M. Crimi, H. Mosbæk, R.L. Siegrist, P.L. Bjerg, Critical reviews in in situ chemical oxidation of contaminated soil and groundwater using persulfate: a review, Environ. Sci. Technol. 40 (2010) 55–91.
[18] A. Long, Y. Lei, H. Zhang, In situ chemical oxidation of organic contaminated soil and groundwater using activated persulfate process, Prog. Chem. 26 (2014) 898–908.
[19] K. Huang, Z. Zhao, G.E. Hoag, A. Dahmani, P.A. Block, Degradation of volatile organic compounds with thermally activated persulfate oxidation, Chemosphere 61 (2005) 551–560.
[20] D. Zhao, X. Liao, X. Yan, S.G. Huling, T. Chai, H. Tao, Effect and mechanism of persulfate activated by different methods for PAHs removal in soil, J. Hazard. Mater. 254–255 (2013) 228–235.
[21] C. Liang, C.J. Bruell, Thermally activated persulfate oxidation of trichloroethylene: experimental investigation of reaction orders, Ind. Eng. Chem. Res. 47 (2008) 2912–2918.
[22] A. Ghauch, A. Tuqan, Oxidation of bisoprolol in heated persulfate/H_2O systems: kinetics and products, Chem. Eng. J. 183 (2012) 162–171.
[23] A. Ghauch, A. Tuqan, N. Kibbi, Ibuprofen removal by heated persulfate in aqueous solution: a kinetics study, Chem. Eng. J. 197 (2012) 483–492.

[24] A. Ghauch, G. Ayoub, S. Naim, Degradation of sulfamethoxazole by persulfate assisted micrometric Fe^0 in aqueous solution, Chem. Eng. J. 228 (2013) 1168–1181.
[25] G. Ayoub, A. Ghauch, Assessment of bimetallic and trimetallic iron-based systems for persulfate activation: application to sulfamethoxazole degradation, Chem. Eng. J. 256 (2014) 280–292.
[26] A. Ghauch, A. Tuqan, N. Kibbi, S. Geryes, Methylene blue discoloration by heated persulfate in aqueous solution, Chemical Eng. J. 213 (2012) 259–271.
[27] X.R. Xu, X.Z. Li, Degradation of azo dye Orange G in aqueous solutions by persulfate with ferrous ion, Sep. Purif. Technol. 72 (2010) 105–111.
[28] I.M. Kolthoff, I.K. Miller, The chemistry of persulfate. I. The kinetics and mechanism of the decomposition of the persulfate ion in aqueous medium, J. Am. Chem. Soc. 73 (1951) 3055–3059.
[29] D.A. House, Kinetics and mechanism of oxidations by peroxydisulfate, Chem. Rev. 62 (1962) 185–203.
[30] X. Xu, S. Li, Q. Hao, J. Liu, Y. Yu, H. Li, Activation of persulfate and its environmental application, Int. J. Environ. Bioeng. 1 (2012) 60–81.
[31] C. Liang, C.F. Huang, N. Mohant, R.M. Kurakalva, A rapid spectrophotometric determination of persulfate anion in ISCO, Chemosphere 73 (2008) 1540–1543.
[32] C. Tan, N. Gao, Y. Deng, W. Rong, S. Zhou, N. Lu, Degradation of antipyrine by heat activated persulfate, Sep. Purif. Technol. 109 (2013) 122–128.
[33] T. Ishimoto, R. Nagumo, T. Ogura, T. Ishihara, B. Kim, A. Miyamoto, M. Koyamaa, Chemical degradation mechanism of model compound, $CF_3(CF_2)_3O(CF_2)_2OCF_2SO_3H$, of PFSA polymer by attack of hydroxyl radical in PEMFCs, J. Electrochem. Soc. 157 (2010) B1305–B1309.
[34] K. Kümmerer, M. Meyer, T. Steger-Hartmann, Biodegradability of the anti-tumor agent ifosfamide and its occurrence in hospital effluents and communal sewage, Water Res. 31 (1997) 2705–2710.
[35] E. Emmanuel, Y. Perrodin, G. Keck, J.M. Blanchard, P. Vermande, Effect of Hospital Wastewater on Aquatic Ecosystem, XXVIII Congreso Interamericano de Ingeniería Sanitaria y Ambiental, Cancún, México, 2002. 1–7.
[36] B. Pauwels, W. Verstraete, The treatment of hospital wastewater: an appraisal, J. Water Health 04 (4) (2006) 405–416.
[37] G.P. Anipsitakis, D.D. Dionysiou, M.A. Gonzalez, Cobalt-mediated activation of peroxymonosulfate and sulfate radical attack on phenolic compounds: implications of chloride ions, Environ. Sci. Technol. 40 (2006) 1000–1007.
[38] E. Marco-Urrea, M. Pérez-Trujill, P. Blánquez, T. Vicent, G. Caminal, Biodegradation of the analgesic naproxen by Trametes versicolor and identification of intermediates using HPLC–DAD–MS and NMR, Bioresour. Technol. 101 (2010) 2159–2166.
[39] G.P. Anipsitakis, D.D. Dionysiou, Radical generation by the interaction of transition metals with common oxidants, Environ. Sci. Technol. 38 (2004) 3705–3712.
[40] P. Neta, V. Madhavan, H. Zemel, R. Fessenden, Rate constants and mechanism of reaction of $SO_4^{\cdot}$ with aromatic compounds, J. Am. Chem. Soc. (1977) 163–164.
[41] A.K. Klefah, M. Eriksson, L.A. Eriksson, Theoretical study of the phototoxicity of naproxen and the active form of nabumetone, J. Phys. Chem. A 112 (2008) 10921–10930.
[42] M.B. Cunha-Santino, I. Bianchini-Júnior, Humic substances mineralization: the variation of pH, electrical conductivity and optical density, Acta Limnol. Bras. 16 (2004) 63–75.
[43] P. Rao, M.S.H. Mak, T. Liu, K.C.K. Lai, I.M.C. Lo, Effects of humic acid on arsenic(V) removal by zero-valent iron from groundwater with special references to corrosion products analyses, Chemosphere 75 (2009) 156–162.
[44] H.V. Lutze, N. Kerlin, T.C. Schmidt, Sulfate radical-based water treatment in presence of chloride: formation of chlorate, inter-conversion of sulfate radicals into hydroxyl radicals and influence of bicarbonate, Water Res. (2014), http://dx.doi.org/10.1016/j.watres.2014.10.006.
[45] P. Neta, R.E. Huie, A.B. Ross, Rate constants for reactions of inorganic radicals in aqueous solutions, J. Phys. Chem. Ref. Data 17 (1988) 1027.
[46] G.G. Jayson, B.J. Parsons, Some simple, highly reactive, inorganic chlorine derivatives in aqueous solution, J. Chem. Soc., Faraday Trans. I (69) (1973) 1597–1607.
[47] B. Venkatachalapathy, P. Ramamurthy, Reactions of nitrate radical with amino acids in acidic aqueous medium: a flash photolysis investigation, J. Photochem. Photobiol., A 93 (1996) 1–5.
[48] G.V. Buxton, A.J. Elliott, Rate constant for reaction of hydroxyl radicals with bicarbonate ions, Radiat. Phys. Chem. 27 (1986) 241–243.
[49] W. Cory, A. DeSantis, C. Ulmer, Photodegradation of naproxen and ibuprofen and the formation of ecotoxic photoproducts in natural water systems. IWA specialty conference on Natural Organic Matter, Costa Mesa, CA, USA, July 27–29, 2011.
[50] E. Arany, R.K. Szabó, L. Apáti, T. Alapi, I. Ilisz, P. Mazellier, A. Dombi, K. Gajda-Schrantz, Degradation of naproxen by UV, VUV photolysis and their combination, J. Hazard. Mater. 262 (2013) 151–157.
[51] S. Selkea, M. Scheurella, M.R. Shahb, H. Hühnerfussa, Identification and enantioselective gas chromatographic mass-spectrometric separation of O-desmethylnaproxen, the main metabolite of the drug naproxen, as a new environmental contaminant, J. Chromatogr. A 1217 (2010) 419–423.
[52] X. Wu, X. Gu, S. Lu, M. Xu, X. Zang, Z. Miao, Z. Qiu, Q. Sui, Degradation of trichloroethylene in aqueous solution by persulfate activated with citric acid chelated ferrous ion, Chem. Eng. J. 255 (2014) 585–592.
[53] M.C.R. Cockett, H. Ozeki, K. Okuyama, K. Kimura, Vibronic coupling in the ground cationic state of naphthalene: a laser threshold photoelectron [zero kinetic energy (ZEKE)-photoelectron] spectroscopic study, J. Chem. Phys. 98 (1993) 7763.
[54] I. Watanabe, Y. Yokoyama, S. Ikeda, Lone pair ionization potentials of carboxylic acids determined by He(I) photoelectron spectroscopy, B. Chem. Soc. Jpn. 46 (1973) 1959–1963.
[55] C. Gadipelly, A. Pérez-González, G.D. Yadav, I. Ortiz, R. Ibáñez, V.K. Rathod, K.V. Marathe, Pharmaceutical industry wastewater: review of the technologies for water treatment and reuse, Ind. Eng. Chem. Res. 53 (2014) 11571–11592.